

DEUTSCHES ELEKTRONEN-SYNCHROTRON
Ein Forschungszentrum der Helmholtz-Gemeinschaft



DESY 20-059
TTP-2020-017
P3H-20-013
arXiv:2004.14852
April 2020

Phenomenology of a Supersymmetric Model Inspired by Inflation

W. G. Hollik

Institut für Kernphysik, Karlsruher Institut für Technologie
and

Institut für Theoretische Teilchenphysik,
Karlsruher Institut für Technologie

C. Li, S. Paasch

Deutsches Elektronen-Synchrotron DESY, Hamburg

G. Moortgat-Pick

II. Institut für Theoretische Physik, Universität Hamburg
and

Deutsches Elektronen-Synchrotron DESY, Hamburg

ISSN 0418-9833

NOTKESTRASSE 85 - 22607 HAMBURG

DESY behält sich alle Rechte für den Fall der Schutzrechtserteilung und für die wirtschaftliche Verwertung der in diesem Bericht enthaltenen Informationen vor.

DESY reserves all rights for commercial use of information included in this report, especially in case of filing application for or grant of patents.

To be sure that your reports and preprints are promptly included in the
HEP literature database
send them to (if possible by air mail):

DESY Zentralbibliothek Notkestraße 85 22607 Hamburg Germany	DESY Bibliothek Platanenallee 6 15738 Zeuthen Germany
---	---

Phenomenology of a Supersymmetric Model Inspired by Inflation

Wolfgang Gregor Hollik^{a,b}, Cheng Li^c, Gudrid Moortgat-Pick^{d,c}, Steven Paasch^c

^a*Institute for Nuclear Physics, Karlsruhe Institute of Technology,
D-76021 Karlsruhe, Germany*

^b*Institute for Theoretical Particle Physics, Karlsruhe Institute of Technology,
D-76128 Karlsruhe, Germany*

^c*DESY, Notkestraße 85, D-22607 Hamburg, Germany*

^d*II. Institut für Theoretische Physik, Universität Hamburg,
Luruper Chaussee 149, D-22761 Hamburg, Germany*

wolfgang.hollik@kit.edu, cheng.li@desy.de,
gudrid.moortgat-pick@desy.de, steven.paasch@desy.de

May 1, 2020

The current challenges in High Energy Physics and Cosmology are to build coherent particle physics models to describe the phenomenology at colliders in the laboratory and the observations in the universe. From these observations, the existence of an inflationary phase in the early universe gives guidance for particle physics models. We study a supersymmetric model which incorporates successfully inflation by a non-minimal coupling to supergravity and shows a unique collider phenomenology. Motivated by experimental data, we set a special emphasis on a new singlet-like state at 97 GeV and single out possible observables for a future linear collider that permit a distinction of the model from a similar scenario without inflation. We define a benchmark scenario that is in agreement with current collider and Dark Matter constraints, and study the influence of the non-minimal coupling on the phenomenology. Measuring the singlet-like state with high precision on the percent level seems to be promising for resolving the models, even though the Standard Model-like Higgs couplings deviate only marginally. However, a hypothetical singlet-like state with couplings of about 20 % compared to a Standard Model Higgs at 97 GeV encourages further studies of such footprint scenarios of inflation.

Contents

1	Introduction	2
2	Theoretical Framework	3
2.1	Higgs sector	4
2.2	Gaugino and chargino sector	7
3	Phenomenological discussion	8
3.1	NMSSM benchmark points	8
3.2	μ NMSSM study of the effects from μ_{inf}	9
3.3	Reweighting μ_{inf} effects in the spectrum	13
4	Conclusions	17
	References	20

1 Introduction

Supersymmetry (SUSY) remains a valid conceptual extension beyond the Standard Model (SM) of particle physics, although there have not yet been any direct signs of superpartners detected in proton–proton collisions even at 13 TeV center of mass energy at the run 2 of the Large Hadron Collider (LHC). However, even light SUSY cannot be experimentally excluded in the electroweak sector. The concept of SUSY as a space-time symmetry is mathematically sound, phenomenologically beautiful and connects the fundamental forces of the SM with gravity. In supergravity, moreover, a non-minimal gravitational coupling of the Higgs particle content leads to a successful embedding of inflation in the early universe [1–4]. The basic Higgs phenomenology of this variation of a Next-to-Minimal Supersymmetric Standard Model (NMSSM) has been described in some detail in [5], where it has been argued, that the main effect of the non-minimal supergravity coupling might be visible in a precise study of a singlet-like Higgs state that has to be discovered at the LHC or future lepton colliders.

Especially the option of a light additional Higgs state as favoured by some observational hints at the Large Electron–Positron Collider (LEP) [6–8] and the LHC [9–11], which can be present in many singlet extended models [12–23], is an intriguing case study also for the inflation-inspired model. We want to state that the existence or nonexistence of such a light Higgs at 97 GeV is neither unique to the model which is going to be studied in the current work, nor is it a special feature of that model.¹ However, it is interesting to connect to new light bosons as they could be studied with unprecedented precision in future e^+e^- -colliders, for instance at the International Linear Collider (ILC) with an initial low center of mass energy of 250 GeV. Thus, we are going to put special emphasis on the e^+e^- -collider phenomenology of a benchmark point which comprises such a scalar boson below 100 GeV.

This paper is structured as follows: First, we briefly review the supersymmetric model motivated by inflation in Sec. 2 which has been introduced in Refs. [2, 3]. The electroweak phenomenology, the Higgs and electroweakino sector has already been discussed in detail in Ref. [5] to which we closely relate here. Second, we perform a parameter scan of the relevant model parameters from where we extract a benchmark scenario which is discussed in more detail in Sec. 3 and discuss the phenomenology of such a scenario. Finally, we conclude in Sec. 4.

¹ Especially the existence of a singlet-like Higgs state below 125 GeV can be present in certain parameter regions of the NMSSM, see Ref. [24].

2 Theoretical Framework

The model with successful early universe inflation in the context of superconformal supergravity [2–4] can be embedded in the general NMSSM (GNMSSM) as reviewed in Ref. [25]. In order to drive inflation, a non-minimal coupling of a Higgs bilinear to gravity is needed, which has been shown to be the gauge invariant product $\hat{H}_u \cdot \hat{H}_d$ as pointed out in Ref. [1]. The singlet superfield is needed to stabilise the inflationary direction [2–4]. At low (electroweak) energies, the superpotential is given by the superpotential of the \mathbb{Z}_3 -invariant NMSSM plus an additional μ -term like in the Minimal Supersymmetric Standard Model (MSSM) $\mu \hat{H}_u \cdot \hat{H}_d$. This parameter we name for clarity μ_{inf} and the model thus “ μ -extended” NMSSM or short μ NMSSM. In contrast to the \mathbb{Z}_3 -invariant NMSSM, there is no accidental \mathbb{Z}_3 symmetry prohibiting certain terms in the superpotential of the GNMSSM like the μ -term for the two Higgs doublet superfields and the mass and tadpole term for the singlet superfield. The μ -term breaks the \mathbb{Z}_3 symmetry of the NMSSM and thus also non- \mathbb{Z}_3 -invariant terms in the soft SUSY breaking sector are supposed to be present. Nevertheless, due to breaking of the superconformal symmetry by only the gravitational coupling, the superpotential does not introduce the mass and tadpole term for the singlet. The soft breaking terms can always be redefined in a way that only the couplings introduced below are relevant.

The superpotential of the μ NMSSM is given by

$$\mathcal{W}_{\mu\text{NMSSM}} = (\lambda \hat{S} + \mu_{\text{inf}}) \hat{H}_u \cdot \hat{H}_d + \frac{\kappa}{3} \hat{S}^3 + \mathcal{W}_{\text{Yukawa}}, \quad (1)$$

where the extra μ -term is related to the non-minimal supergravity coupling χ via the gravitino mass as $\mu_{\text{inf}} = \frac{3}{2} m_{3/2} \chi$. The Yukawa terms are the same as in the (N)MSSM. Chiral superfields are denoted with a hat, where \hat{H}_u and \hat{H}_d are the up- and down-type Higgs doublet, respectively, and \hat{S} the singlet superfield. The corresponding soft SUSY breaking Lagrangian is given by

$$-\mathcal{L}_{\text{soft}} = \left[A_\lambda \lambda S H_u \cdot H_d + \frac{1}{3} A_\kappa \kappa S^3 + B_\mu \mu H_u \cdot H_d + \text{h. c.} \right] + m_{H_d}^2 |H_d|^2 + m_{H_u}^2 |H_u|^2 + m_s^2 |S|^2. \quad (2)$$

The soft SUSY breaking Higgs masses can be related to the electroweak symmetry breaking conditions and are no free parameters. The B_μ terms play a subdominant role and can be set to zero throughout this work.

After electroweak symmetry breaking, the scalar components of the three Higgs superfields acquire vacuum expectation values (vevs) v_u , v_d and v_s . We expand these fields around the vacuum configuration and write:

$$H_u = \begin{pmatrix} h_u^+ \\ h_u \end{pmatrix} = \begin{pmatrix} \eta_u^+ \\ v_u + \frac{1}{\sqrt{2}}(\sigma_u + i\phi_u) \end{pmatrix}, \quad H_d = \begin{pmatrix} h_d \\ h_d^- \end{pmatrix} = \begin{pmatrix} v_d + \frac{1}{\sqrt{2}}(\sigma_d + i\phi_d) \\ \eta_d^- \end{pmatrix} \\ S = v_s + \frac{1}{\sqrt{2}}(\sigma_s + i\phi_s). \quad (3)$$

The ratio of the two doublet vevs defines the parameter $\tan \beta = v_u/v_d$, where $v = \sqrt{v_u^2 + v_d^2} = 174 \text{ GeV}$ corresponds to the SM-vev. Consequently, v_u and v_d are given by $v_u = v \sin \beta$ and $v_d = v \cos \beta$. The vev of the singlet field S dynamically induces a μ -term which we denote as the *effective* μ -term, $\mu_{\text{eff}} = \lambda v_s$. Although it might be suggestive to combine the two μ -terms as $\mu_{\text{eff}} \rightarrow \mu_{\text{inf}} + \mu_{\text{eff}}$, they lead to different phenomenologies in the Higgs and Neutralino sector, as has been pointed out in Ref. [5].

Thus, we consider both μ_{inf} and μ_{eff} as independent free parameters in our study. The consequent differences in the phenomenology will be the crucial point of our discussion. The Neutralino–Singlino

mixing will also be affected by the interplay of μ_{inf} and μ_{eff} and therewith the character of the contribution to dark matter may vary. Since μ_{inf} is related to the gravitino mass, dark matter might also be pure gravitino dark matter, see the discussion in Ref. [5].

According to the cosmological analysis [3, 4], the value of the non-minimal gravity coupling χ can be estimated to $\chi \simeq 10^5 \lambda$. Thus, with $\lambda > 0$, we also set μ_{inf} to be non-negative.²

2.1 Higgs sector

The superpotential (1) and the soft-breaking Lagrangian (2) together with the usual D -terms (quartic Higgs couplings due to quadratic gauge couplings which do not exist for the singlet) lead to the following scalar Higgs potential (with $B_\mu = 0$):

$$\begin{aligned} V_{\text{Higgs}} = & (m_{H_d}^2 + (\mu_{\text{inf}} + \lambda S)^2) |H_d|^2 + (m_{H_u}^2 + (\mu_{\text{inf}} + \lambda S)^2) |H_u|^2 \\ & + (\kappa S^2 + \lambda H_u \cdot H_d)^2 + \frac{g_2^2}{2} |H_d^\dagger H_u|^2 + \frac{g_1^2 + g_2^2}{8} (|H_d|^2 - |H_u|^2)^2 \\ & + m_S^2 S^2 + 2\lambda A_\lambda S H_u \cdot H_d + \frac{2}{3} \kappa A_\kappa S^3. \end{aligned} \quad (4)$$

The mass terms finally arise from the second derivative with respect to the component fields in Eqs. (2) evaluated at the vacuum. Note that the soft breaking terms $m_{H_u}^2$, $m_{H_d}^2$ and m_S^2 are fixed by the minimisation conditions for electroweak symmetry breaking. For convenience, we list the mass matrix elements of the scalar, pseudoscalar and charged Higgs matrices, M_S^2 , M_P^2 , and M_C^2 , respectively, as worked out in Ref. [5]; we only keep the contribution from μ_{inf} in comparison with the GNMSSM:³

$$M_{S,11}^2 = m_Z^2 \cos^2 \beta + \mu_{\text{eff}} \left(\frac{\kappa}{\lambda} \mu_{\text{eff}} + A_\lambda \right) \tan \beta \quad (5a)$$

$$M_{S,22}^2 = m_Z^2 \sin^2 \beta + \mu_{\text{eff}} \left(\frac{\kappa}{\lambda} \mu_{\text{eff}} + A_\lambda \right) / \tan \beta \quad (5b)$$

$$M_{S,33}^2 = \frac{\lambda^2 v^2}{\mu_{\text{eff}}} (\cos \beta \sin \beta A_\lambda - \mu_{\text{inf}}) + \frac{\kappa}{\lambda} \mu_{\text{eff}} \left(A_\kappa + 4 \frac{\kappa}{\lambda} \mu_{\text{eff}} \right) \quad (5c)$$

$$M_{S,12}^2 = M_{S,21}^2 = (2v^2 \lambda^2 - m_Z^2) \cos \beta \sin \beta - \mu_{\text{eff}} \left(\frac{\kappa}{\lambda} \mu_{\text{eff}} + A_\lambda \right) \quad (5d)$$

$$M_{S,13}^2 = M_{S,31}^2 = \lambda v \left(2(\mu_{\text{eff}} + \mu_{\text{inf}}) \cos \beta - \left(A_\lambda + 2 \frac{\kappa}{\lambda} \mu_{\text{eff}} \right) \sin \beta \right) \quad (5e)$$

$$M_{S,23}^2 = M_{S,32}^2 = \lambda v \left(2(\mu_{\text{eff}} + \mu_{\text{inf}}) \sin \beta - \left(A_\lambda + 2 \frac{\kappa}{\lambda} \mu_{\text{eff}} \right) \cos \beta \right), \quad (5f)$$

² One can always choose $\lambda > 0$ and allow for negative κ .

³ We express in terms of the gauge boson masses

$$m_W^2 = \frac{1}{2} g_2^2 v^2, \quad m_Z^2 = \frac{1}{2} (g_1^2 + g_2^2) v^2.$$

$$M_{P,11}^2 = \mu_{\text{eff}} \left(\frac{\kappa}{\lambda} \mu_{\text{eff}} + A_\lambda \right) \tan \beta \quad (6a)$$

$$M_{P,22}^2 = \mu_{\text{eff}} \left(\frac{\kappa}{\lambda} \mu_{\text{eff}} + A_\lambda \right) / \tan \beta \quad (6b)$$

$$M_{P,33}^2 = \frac{\lambda^2 v^2}{\mu_{\text{eff}}} \left(\left(4 \frac{\kappa}{\lambda} \mu_{\text{eff}} + A_\lambda \right) \cos \beta \sin \beta - \mu_{\text{inf}} \right) - 3 \frac{\kappa}{\lambda} \mu_{\text{eff}} A_\kappa \quad (6c)$$

$$M_{P,12}^2 = M_{P,21}^2 = \mu_{\text{eff}} \left(\frac{\kappa}{\lambda} \mu_{\text{eff}} + A_\lambda \right) \quad (6d)$$

$$M_{P,13}^2 = M_{P,31}^2 = -v\lambda \left(2 \frac{\kappa}{\lambda} \mu_{\text{eff}} - A_\lambda \right) \sin \beta \quad (6e)$$

$$M_{P,23}^2 = M_{P,32}^2 = -v\lambda \left(2 \frac{\kappa}{\lambda} \mu_{\text{eff}} - A_\lambda \right) \cos \beta, \quad (6f)$$

$$M_{C,11}^2 = (m_W^2 - v^2 \lambda^2) \sin^2 \beta + \mu_{\text{eff}} \left(\frac{\kappa}{\lambda} \mu_{\text{eff}} + A_\lambda \right) \tan \beta \quad (7a)$$

$$M_{C,22}^2 = (m_W^2 - v^2 \lambda^2) \cos^2 \beta + \mu_{\text{eff}} \left(\frac{\kappa}{\lambda} \mu_{\text{eff}} + A_\lambda \right) / \tan \beta \quad (7b)$$

$$M_{C,12}^2 = (m_W^2 - v^2 \lambda^2) \sin \beta \cos \beta + \mu_{\text{eff}} \left(\frac{\kappa}{\lambda} \mu_{\text{eff}} + A_\lambda \right). \quad (7c)$$

The pseudoscalar and charged mass matrix comprise one vanishing eigenvalue each. These correspond to the would-be-Goldstone modes. Diagonalisation of those two matrices is easy and can be done with a rotation by the angle β . The charged Higgs mass is then found to be given by the expression:

$$m_{H^\pm}^2 = m_W^2 - v^2 \lambda^2 + \frac{\mu_{\text{eff}}}{\cos \beta \sin \beta} \left(\frac{\kappa}{\lambda} \mu_{\text{eff}} + A_\lambda \right), \quad (8)$$

from which we can resolve for A_λ and use m_{H^\pm} as input parameter to replace the appearance of A_λ in the model. We then can use the relation

$$\mu_{\text{eff}} \left(\frac{\kappa}{\lambda} \mu_{\text{eff}} + A_\lambda \right) = (m_{H^\pm}^2 - m_W^2 + v^2 \lambda^2) \cos \beta \sin \beta \quad (9)$$

to cancel out the κ and μ_{eff} dependences in Eqs. (6f) and (7c). Furthermore, if we fix m_{H^\pm} to a large value $m_{H^\pm}^2 \gg v^2$, the heaviest neutral Higgs bosons both for CP-even and CP-odd case are basically independent of κ , μ_{eff} and μ_{inf} ; *i. e.* the heavy mass eigenvalues are dominantly controlled by m_{H^\pm} . We are in general left with the following free parameters in our study:

$$\tan \beta, \quad \lambda, \quad \kappa, \quad \mu_{\text{eff}}, \quad \mu_{\text{inf}}, \quad A_\kappa, \quad m_{H^\pm}. \quad (10)$$

In the following, we treat both $\tan \beta$ and m_{H^\pm} as fixed input parameters that are kept to some experimentally allowed value. By this choice, the matrix elements $M_{S,P,11}^2$, $M_{S,P,22}^2$ and $M_{S,P,12}^2$ do not vary under variation of the other inputs. We are interested in the effect of the inflation specific parameters, for which $\tan \beta$ and m_{H^\pm} play a subleading role and have rather the same influence as in the usual NMSSM. The further elements $M_{S,P,13}^2$, $M_{S,P,23}^2$ and $M_{S,P,33}^2$ are then mainly controlled by the parameter combinations $\frac{\kappa}{\lambda} \mu_{\text{eff}}$ and the sum $\mu_{\text{eff}} + \mu_{\text{inf}}$ aside from m_{H^\pm} . Thus, the properties of the light neutral Higgs states at tree level are dominated by these two combinations, although the other free parameters λ , A_κ , and μ_{inf} can influence the mass matrices.

From the diagonalisation, we retrieve the Higgs mixing parameters S_{ij} , P_{ij} and C_{ij} for the scalar, pseudoscalar and charged cases, respectively. The diagonal matrices are found as $\tilde{M}_S^2 = \mathbf{S}^\dagger \mathbf{M}_S^2 \mathbf{S}$, $\tilde{M}_P^2 = \mathbf{P}^\dagger \mathbf{M}_P^2 \mathbf{P}$, and $\tilde{M}_C^2 = \mathbf{C}^\dagger \mathbf{M}_C^2 \mathbf{C}$. With the mixing matrices, the Higgs couplings to SM particles can be conveniently expressed and compared to the SM values in terms of “reduced” couplings. So for

example, reduced couplings of the i -th scalar Higgs to bottom and top quarks are given by:

$$\frac{g_{h_i b\bar{b}}}{g_{H_{\text{SM}} b\bar{b}}} = \frac{S_{i1}}{\cos \beta}, \quad \frac{g_{h_i t\bar{t}}}{g_{H_{\text{SM}} t\bar{t}}} = -\frac{S_{i2}}{\sin \beta}, \quad (11)$$

and the reduced coupling to gauge bosons reads:

$$\frac{g_{h_i ZZ}}{g_{H_{\text{SM}} ZZ}} = \frac{g_{h_i W^+ W^-}}{g_{H_{\text{SM}} W^+ W^-}} = \cos \beta S_{i1} + \sin \beta S_{i2}. \quad (12)$$

Note, that in the μNMSSM , as well as the NMSSM , the reduced gauge boson couplings for Z and W are the same at the tree level. In the course of this work, we explicitly focus on the Higgsstrahlung process at lepton colliders, for which the cross section is controlled by the Higgs coupling to vector bosons g_{HVV} .

Although the reduced couplings from above⁴ cannot be directly probed by experiment, they give important information for the production and decay cross sections. In the so-called κ -framework, effective Higgs couplings are determined from measured rates in the relevant channels. The reduced couplings are then found from ratios of cross section times branching ratios. The coupling-strength modifiers κ are not to be identified with the reduced couplings. However, under certain assumptions like a small width the difference is negligible for a leading order analysis. In case the production and decay can be factorised, the coupling modifiers factor out as

$$\sigma(X \rightarrow H) \text{Br}(H \rightarrow f) = \kappa_X^2 \kappa_f^2 \sigma_X^{\text{SM}} \frac{\Gamma_f^{\text{SM}}}{\Gamma_H(\kappa_X^2, \kappa_f^2)}, \quad (13)$$

with the SM production cross section σ_X^{SM} and the partial decay width for the SM Higgs Γ_f^{SM} into a certain final state f . $\Gamma_H(\kappa_X^2, \kappa_f^2)$ is the total width in presence of the coupling modifiers κ_X and κ_f . The individual modified coupling strengths can be found as the ratios

$$\kappa_X^2 = \frac{\sigma_X}{\sigma_X^{\text{SM}}} \quad \text{and} \quad \kappa_f^2 = \frac{\Gamma_f}{\Gamma_f^{\text{SM}}}. \quad (14)$$

Note that in general higher order accuracy is lost and the κ can be more complicated functions of the reduced couplings. The latter is especially important for the modified couplings to gluons and photons [26]. This has to be included in a correct study of the modified couplings.

For our numerical studies, we refer to the `NMSSMTools` package [27–30] as spectrum generator and for calculations of some crucial observables⁵ that are given below. Although `NMSSMTools` does not provide the input for the μNMSSM , but rather the GNMSSM , we can redefine the input parameters in a way that is compatible with the μNMSSM . Note, that in the GNMSSM , out of the three \mathbb{Z}_3 -breaking parameters in the superpotential, one can always be eliminated by redefinition of the others. Since in `NMSSMTools` the input list does not contain the general μ parameter which corresponds to μ_{inf} , we have transferred the effect to the other parameters and redefine the overall inputs by the following

⁴The reduced couplings are defined at tree level. Radiative corrections are implemented in the mixing matrix elements S_{ij} as they are defined from the loop-corrected mass matrices in `NMSSMTools`.

⁵We are using the highest possible precision implemented in `NMSSMTools` for the GNMSSM : full one loop top/bottom contribution plus leading logarithmic two loop top/bottom and leading logarithmic one loop electroweak corrections [31].

replacement list:

$$\mu_{\text{eff}} \rightarrow \mu_{\text{eff}} + \mu_{\text{inf}}, \quad (15a)$$

$$\kappa \rightarrow \kappa \frac{\mu_{\text{eff}}}{\mu_{\text{eff}} + \mu_{\text{inf}}}, \quad (15b)$$

$$\mu' \rightarrow 0, \quad (15c)$$

$$\xi_F \rightarrow 0, \quad (15d)$$

$$\xi_S \rightarrow \frac{\lambda}{\mu_{\text{eff}}} (v^2 \mu_{\text{inf}} (\mu_{\text{eff}} + \mu_{\text{inf}}) - v_u v_d A_\lambda \mu_{\text{inf}}), \quad (15e)$$

$$m_3^2 \rightarrow -\mu_{\text{inf}} (A_\lambda + \frac{\kappa}{\lambda} \mu_{\text{eff}}), \quad (15f)$$

$$m_S^{\prime 2} \rightarrow -2 \frac{\kappa \lambda \mu_{\text{inf}}}{\mu_{\text{eff}} + \mu_{\text{inf}}} v_u v_d. \quad (15g)$$

By this redefinitions, also the additional soft-breaking terms are involved and thus all effects and arising singularities in the quantum corrections are appropriately taken care of. The superpotential parameters μ' and ξ_F , cf. Ref. [25], are protected by supersymmetry and can be set to zero at all scales.⁶

2.2 Gaugino and chargino sector

In the μ NMSSM, the Higgsino mass parameter is given by $(\mu_{\text{eff}} + \mu_{\text{inf}})$ instead of μ_{eff} in the NMSSM. In contrast to the NMSSM, however, the singlino mass is driven by a different combination. The symmetric mass matrices for neutralinos and charginos are given by (see *e. g.* Ref. [5] and references therein)

$$M_{\tilde{\chi}^0} = \begin{pmatrix} M_1 & 0 & -m_Z \sin \theta_w \cos \beta & m_Z \sin \theta_w \sin \beta & 0 \\ \cdot & M_2 & m_Z \cos \theta_w \cos \beta & -m_Z \cos \theta_w \sin \beta & 0 \\ \cdot & \cdot & 0 & -(\mu_{\text{inf}} + \mu_{\text{eff}}) & -\lambda v \sin \beta \\ \cdot & \cdot & \cdot & 0 & -\lambda v \cos \beta \\ \cdot & \cdot & \cdot & \cdot & 2 \frac{\kappa}{\lambda} \mu_{\text{eff}} \end{pmatrix}, \quad (16)$$

$$M_{\tilde{\chi}^\pm} = \begin{pmatrix} M_2 & \sqrt{2} m_W \sin \beta \\ \sqrt{2} m_W \cos \beta & \mu_{\text{inf}} + \mu_{\text{eff}} \end{pmatrix}, \quad (17)$$

where θ_w is the weak mixing angle and $M_{1,2}$ the soft SUSY breaking gaugino masses for the bino and wino, respectively. The matrices are given in the basis of gauge eigenstates, where:

$$(\tilde{\psi}^0)^T = (\tilde{B}^0, \tilde{W}_3^0, \tilde{h}_d^0, \tilde{h}_u^0, \tilde{s}^0), \quad (\tilde{\psi}^+)^T = (\tilde{W}^+, \tilde{h}_u^+) \quad \text{and} \quad (\tilde{\psi}^-)^T = (\tilde{W}^-, \tilde{h}_d^-), \quad (18)$$

with the bino \tilde{B}^0 , the neutral and charged wino components \tilde{W}_3^0 and \tilde{W}^\pm , the charged and neutral higgsino components $\tilde{h}_{u,d}^\pm$ and $\tilde{h}_{u,d}^0$, and the singlino component \tilde{s}^0 . The mass eigenstates are denoted by the neutralinos $\tilde{\chi}_{1-5}^0$ and charginos $\tilde{\chi}_{1,2}^\pm$.

One can see that the mass of the higgsino component is driven by the sum $\mu_{\text{inf}} + \mu_{\text{eff}}$, while the mass scale of the singlino component is driven by $\frac{\kappa}{\lambda} \mu_{\text{eff}}$. Since the singlino mass is the only matrix element that contains the parameter κ at the tree level, one may use this to reweight any relative shift between μ_{eff} and μ_{inf} by a change of κ in order to keep the neutralino spectrum under variation of μ_{inf} . This rescaling procedure has been described in Ref. [5] and will be also used in the following to tackle the

⁶ The notation of the GNMSSM parameters in Ref. [5] is $\mu' = \nu$, $\xi_F = \xi$, $\xi_S = \xi C_\xi$, $m_3^2 = \mu B_\mu$, $m_S^{\prime 2} = \nu B_\nu$.

Table 1: Fixed SM and SUSY input parameters of the NMSSM scenario. The gaugino mass parameters are denoted as M_i with $i = 1, 2, 3$ and the ratio of the electroweak vevs $\tan\beta$. We have the trilinear soft-breaking sfermion term A_{f_3} , the sfermion mass $m_{\bar{f}_L, \bar{f}_R}$ and also the charged Higgs mass input M_{H^\pm} .

$m_Z = 91.187 \text{ GeV}$	$\alpha_{\text{em}}^{-1} = 127.92$	$G_F = 1.16637 \cdot 10^{-5} \text{ GeV}^{-2}$		
$M_1 = 239 \text{ GeV}$	$M_2 = 500 \text{ GeV}$	$M_3 = 2500 \text{ GeV}$		
$m_{\bar{f}_L, \bar{f}_R} = 2000 \text{ GeV}$	$A_{f_3} = 3000 \text{ GeV}$	$\tan\beta = 12$	$M_{H^\pm} = 2000 \text{ GeV}$	

effect of μ_{inf} in the model.

3 Phenomenological discussion

In this section we explore methods to experimentally distinguish the NMSSM from the μ NMSSM. For this purpose, we perform a scan in the NMSSM parameter space and select points passing a number of experimental constraints. Based on one benchmark scenario we scan the μ NMSSM parameter space for points with a similar mass spectrum within an interval of a few GeV. We discuss experimental observables like branching ratios and cross-sections to describe features introduced by the parameter space of the μ NMSSM. Starting from the NMSSM benchmark point, we show the effect from μ_{inf} exclusively and the option to conceal the influence from this parameter by a redefinition of others. Finally, we discuss methods to experimentally distinguish both models.

3.1 NMSSM benchmark points

A full phenomenological discussion of the complete parameter space in the μ NMSSM and NMSSM is a formidable task. We want to focus on a certain feature in the Higgs mass spectrum comprising a light neutral scalar boson. In order to achieve this, we have scanned for points in the NMSSM parameter space having this feature and passing the constraints given by `NMSSMTools` version 5.5.2 [27, 28, 32] (*e.g.* certain collider observables and Dark Matter constraints), as well as `HiggsBounds` version 5.3.2 [33, 34], `HiggsSignals` version 2 [35, 36], and `CheckMATE` version 2.0.26 [37–43] for LHC analyses. For the scan, we have constrained ourselves to a variation of relevant parameters only, where we keep less relevant SUSY parameters at fixed values.⁷ The values of all fixed parameters are given in Tab. 1. Besides the SM parameters, we keep the gaugino mass parameters M_1 and M_2 obeying the GUT relation $M_1 = \frac{5}{3} \frac{g_1^2}{g_2^2} M_2$ with $M_2 = 500 \text{ GeV}$. The gluino mass M_3 is fixed to 2500 GeV, the sfermion soft-breaking trilinear terms A_{f_3} to 1200 GeV and all the sfermion masses $m_{\bar{f}_L, \bar{f}_R}$ to 2000 GeV.

`NMSSMTools` uses `NMHCAY` [27, 32] to compute the masses, couplings and decay widths of all Higgs bosons and the masses of all other sparticles. The Higgs spectrum is calculated with the highest available precision for the GNMSSM implemented in `NMSSMTools`, containing one loop and leading logarithmic two loop corrections with top and bottom Yukawa couplings, and leading logarithmic electroweak corrections, using the pole mass scheme. For each point, `NMSSMTools` calculates the NMSSM spectrum, where we vary the input values of the couplings κ , λ , and the soft SUSY-breaking parameter A_κ , as well as μ_{eff} . We have chosen to scan λ and κ between 0 and 0.1 each; $|\mu_{\text{eff}}|$ from 100 GeV to 1000 GeV; and A_κ between -300 GeV and 300 GeV . Note that the absence of tachyons in

⁷ Relevant for the study of μ_{inf} in the Higgs sector.

the spectrum usually requires $\text{sign } A_\kappa \neq \text{sign } \mu_{\text{eff}}$; we excluded small absolute values of μ_{eff} to avoid direct exclusion limits from LEP for light charginos.

In our scan, we have calculated the Dark Matter relic density and direct detection rates as well as indirect detection constraints with `NMSSMTools` using `micrOMEGAs` [44–46]. Furthermore, many observables are calculated and compared with experimental bounds from LEP and LHC by `NMSSMTools`. Points passing these constraints have then been checked with `HiggsBounds` for 95% C.L. exclusion at LEP, Tevatron and LHC; furthermore the SM-like Higgs properties have been tested with `HiggsSignals`. We take special emphasis on the Higgsstrahlung process $e^+e^- \rightarrow h_1 Z$ which has been important at LEP and will play the same role at the ILC. The cross section is controlled by the Higgs coupling to gauge bosons displayed in Eq. (12). Finally we have employed `CheckMATE` to test for current exclusions from Drell–Yan production at the LHC, as well as neutralino production $pp \rightarrow \tilde{\chi}_1^0 \tilde{\chi}_1^0$, $pp \rightarrow \tilde{\chi}_1^0 \tilde{\chi}_2^0$ and chargino production $pp \rightarrow \tilde{\chi}_1^+ \tilde{\chi}_1^-$. `CheckMATE` simulates signal events for BSM models at the LHC and compares with the data from the experimental analyses for exclusion. As a result, a criterion is provided by `CheckMATE` which is used to determine whether the parameter point is disfavoured or not. This criterion is the r value which is defined by the ratio between the number of simulated signal events S and the 95% upper limit of experimental data S_{95} :

$$r = \frac{S - 1.96 \cdot \Delta S}{S_{95}}. \quad (19)$$

If $r > 1$, the BSM prediction exceeds the 95% C.L. and the model is excluded. Moreover, we calculated cross sections for light Higgs production $e^+e^- \rightarrow Z h_{1,2}$ using `MadGraph5` version 2.7.2. We have identified a benchmark point passing all experimental constraints implemented in the codes listed above which comprises a light Higgs at 97 GeV.

The full mass spectrum of the Higgs, neutralino and chargino sector is shown in Tab. 2. The lightest Higgs has a mass $m_{h_1} = 96.99$ GeV, where the SM-like Higgs $m_{h_2} = 125.3$ GeV. We have accepted SM-like Higgs masses within the ranges $m_{h_{\text{SM}}} = (125.1 \pm 3)$ GeV. The heavy \mathcal{CP} -even, \mathcal{CP} -odd and charged Higgs H_3 , A and H^\pm have masses $\lesssim 2000$ GeV as defined by the input value of Tab. 1. The neutralino sector is found to be quite heavy with the lightest neutralino at ~ 190 GeV. However, the second to fourth lightest neutralinos $\tilde{\chi}_{2\dots 4}$ are very close in mass to $\tilde{\chi}_1^0$ between $m_{\tilde{\chi}_2} = 194.2$ GeV and $m_{\tilde{\chi}_4} = 255.1$ GeV. The lightest chargino has a mass of $m_{\tilde{\chi}_1^\pm} = 214.5$ GeV while the second chargino has the same mass as the heaviest neutralino, $m_{\tilde{\chi}_2^\pm} \approx 2m_{\tilde{\chi}_5^0}$. The input parameters of this point as result of the scan are shown in Tab. 3. The negative μ_{eff} can be traded for a negative A_κ without much change. Note, that the large $A_\kappa \simeq 270$ GeV is responsible for a heavy \mathcal{CP} -odd singlet with $m_a = 273.7$ GeV in contrast to its lighter \mathcal{CP} -even counterpart.

3.2 μ NMSSM study of the effects from μ_{inf}

Starting from the benchmark point discussed above, we are interested to see the effect of μ_{inf} . The NMSSM limit is reached for $\mu_{\text{inf}} = 0$ GeV. We increase the value of μ_{inf} from 0 to 1000 GeV and study how the spectrum is changed, how the mixing is affected, and finally how the phenomenology (reduced couplings and branching ratios) of the light Higgs states vary under modulation of μ_{inf} . All the other parameters are kept the same.

We show the spectrum of the light \mathcal{CP} -even Higgs bosons $h_{1,2}$ and the light \mathcal{CP} -odd state a , as well as the light neutralinos and charginos in Fig. 1. For $\mu_{\text{inf}} = 0$ GeV we recover the NMSSM spectrum given in Tab. 2, where around $\mu_{\text{inf}} = 200$ GeV the mass of the light Higgs h_1 turns into a tachyonic dip where no line is shown and finally rises again towards $\mu_{\text{inf}} \simeq 348$ GeV where it reaches a second maximum. At around $\mu_{\text{inf}} \approx 210$ GeV, the combination $\mu_{\text{eff}} + \mu_{\text{inf}}$ is close to zero, which drives the tachyonic behaviour. The first maximum, corresponding to the first minimum of m_{h_2} is around $\mu_{\text{inf}} = 46$ GeV.

Table 2: Mass spectrum of our NMSSM point. In the Higgs sector we have the lightest scalar Higgs h_1 , the SM-like Higgs h_2 , the Heavy Higgs H_3 , as well as the \mathcal{CP} -odd Higgses a and A and the charged Higgs H^\pm . The neutralino sector is labeled with $\tilde{\chi}_{1\dots 5}$, and the chargino masses are denoted as $m_{\tilde{\chi}_{1,2}^\pm}$.

$m_{h_1} = 96.99 \text{ GeV}$	$m_{h_2} = 125.3 \text{ GeV}$	$m_{H_3} = 1962 \text{ GeV}$
$m_a = 273.7 \text{ GeV}$	$m_A = 1962 \text{ GeV}$	$m_{H^\pm} = 1964 \text{ GeV}$

$m_{\tilde{\chi}_1^0} = 190.4 \text{ GeV}$	$m_{\tilde{\chi}_2^0} = 194.2 \text{ GeV}$	$m_{\tilde{\chi}_3^0} = 226.1 \text{ GeV}$
$m_{\tilde{\chi}_4^0} = 255.1 \text{ GeV}$	$m_{\tilde{\chi}_5^0} = 538.3 \text{ GeV}$	
$m_{\tilde{\chi}_1^\pm} = 214.5 \text{ GeV}$	$m_{\tilde{\chi}_2^\pm} = 538.3 \text{ GeV}$	

Table 3: Results for the parameter scan in the NMSSM with μ_{eff} at the electroweak scale, the soft SUSY-breaking parameter A_κ and the couplings κ and λ leading to the mass spectrum shown in Tab. 2.

$\mu_{\text{eff}} = -212.3 \text{ GeV}$	$A_\kappa = 268.6 \text{ GeV}$
$\kappa = 0.01846$	$\lambda = 0.04215$

In contrast to this rich evolution of $m_{h_{1,2}}$ with μ_{inf} , the mass of a varies only mildly and is dominated by the fixed value of A_κ . On the right hand side of Fig. 1, we show the light neutralino masses evolving with μ_{inf} . In the regime below 400 GeV, all three displayed masses behave linearly with μ_{inf} , where for larger $\mu_{\text{inf}} \gtrsim 400 \text{ GeV}$ the dominant wino-, bino-, and singlino-like behaviour is developed. The linearly rising mass with μ_{inf} belongs to higgsino-like states, as their mass is mainly driven by $\mu_{\text{eff}} + \mu_{\text{inf}}$. The singlino, in contrast is supposed to stay constant under variation of μ_{inf} as can be seen from the mass matrix in Eq. (16), where $(M_{\tilde{\chi}^0})_{55} = 2\frac{\kappa}{\lambda}\mu_{\text{eff}} = -185.958 \text{ GeV}$ for the parameters in this scenario given in Tab. 3. This shows how differently the spectra of Higgs bosons and neutralinos/charginos evolve with μ_{inf} . Although there are three distinct values of μ_{inf} where the Higgs spectrum essentially looks the same as for the NMSSM point, for two of them the neutralinos become much lighter and thus in conflict with Dark Matter phenomenology. We have identified one point at $\mu_{\text{inf}} \simeq 395 \text{ GeV}$ which comprises the same spectra for both Higgs and neutralino/chargino as for $\mu_{\text{inf}} = 0 \text{ GeV}$.

Crucial for the phenomenology of this scenario is a view on the Higgs mixing matrices, especially the singlet-doublet mixings as shown in Fig. 2. Here, we show the singlet admixture to the lightest state (left side top), and the doublet components of the same (left side middle and down). On the right hand side, the same is shown for the second lightest state. It is interesting to see that there are two degenerate points, where h_1 is purely singlet and h_2 purely doublet. These points coincide with the minima and maxima in the spectrum of Fig. 1. Towards large values of μ_{inf} , the second lightest Higgs becomes singlet-dominated, while the lightest loses its singlet character. Note, however, that there is no scalar at 125 GeV in the spectrum anymore, so the regime of large μ_{inf} is disfavoured by observations.

The Higgs mixing also defines the reduced couplings at the tree level, see Eqs. (11) and (12). The

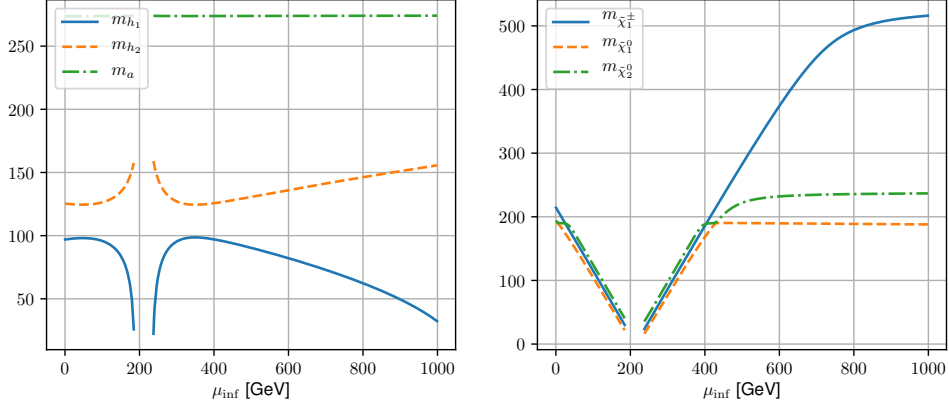


Figure 1: The masses of scalar higgses h_1 , h_2 , pseudoscalar higgs a , neutralinos $\tilde{\chi}_1^0$, $\tilde{\chi}_2^0$, and chargino $\tilde{\chi}_1^\pm$, depending on μ_{inf} .

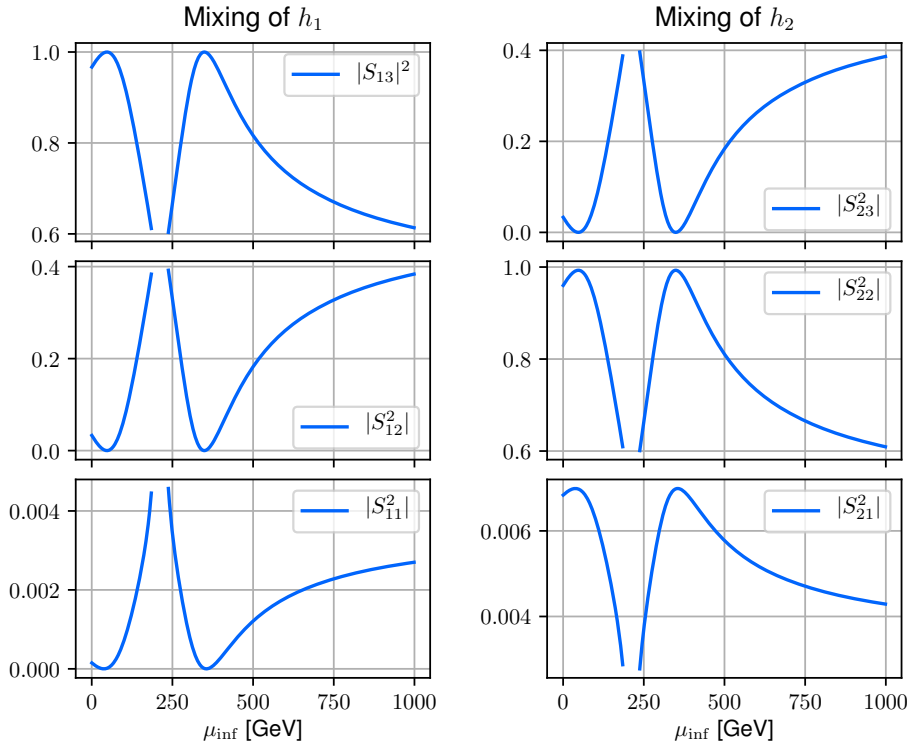


Figure 2: The three mixing components of two lightest Higgs bosons depending on μ_{inf} . The down type components are $|S_{11}^2|$ and $|S_{21}|^2$, the up type components are $|S_{12}|^2$ and $|S_{22}|^2$, and the singlet components are $|S_{13}|^2$ and $|S_{23}|^2$.

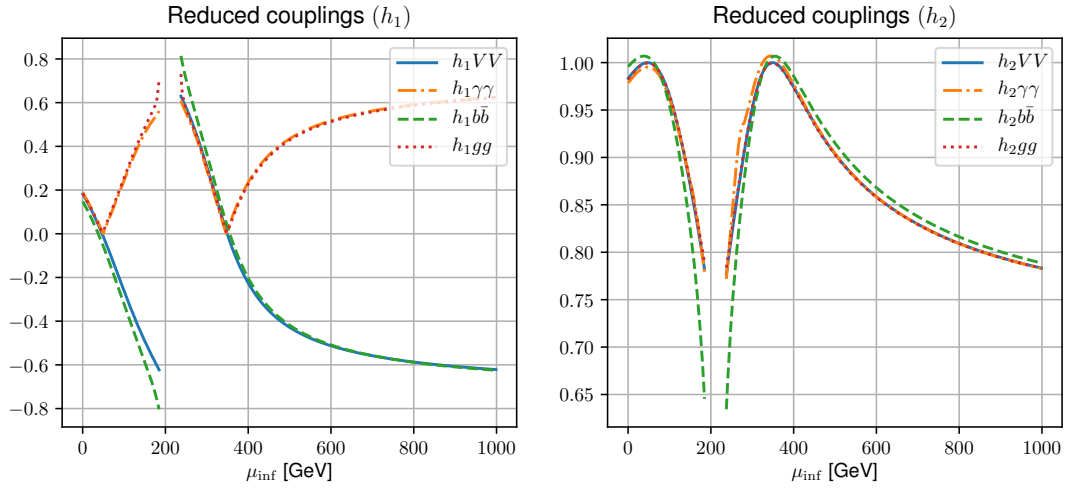


Figure 3: The reduced couplings of h_1 and h_2 to gauge bosons, photons, b quarks and gluons, depending on μ_{inf}

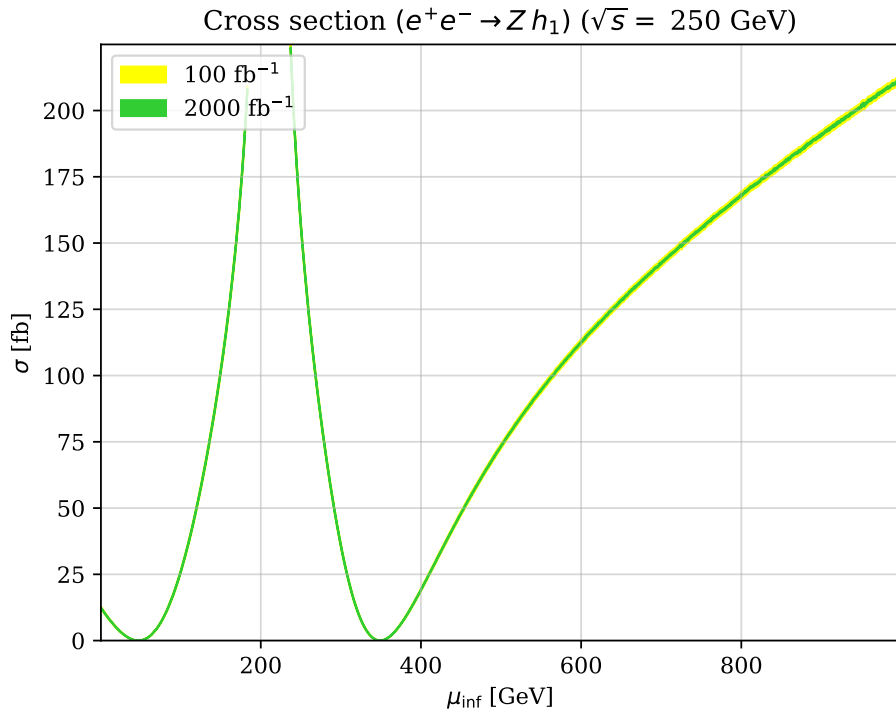


Figure 4: The lightest scalar Higgs production cross section at 250 GeV ILC depending on μ_{inf}

reduced couplings as delivered by `NMSSMTools` are shown in Fig. 3, where we display the reduced couplings to electroweak gauge bosons (VV), photons ($\gamma\gamma$), bottom quarks ($b\bar{b}$), and gluons (gg) for the lightest and second lightest Higgs, h_1 and h_2 respectively. It can be seen that for the two points mentioned above with $\mu_{\text{inf}} \simeq 46$ GeV and $\simeq 348$ GeV the reduced couplings of h_2 approach the SM values, where in contrast the couplings of h_1 turn to zero. This is exactly the pure singlet case. In the neighbouring regime, the singlet-like state has small couplings to the SM and the couplings of h_2 deviate from the SM values. It is furthermore interesting to notice that the reduced couplings of the lightest state h_1 to gauge bosons and bottom quarks have the same absolute value but opposite signs in the regime $46 \text{ GeV} \lesssim \mu_{\text{inf}} \lesssim 348 \text{ GeV}$. This gives a handle to distinguish finally the two degenerate spectra for different values of μ_{inf} . Especially for the point degenerate with the NMSSM case as discussed above for $\mu_{\text{inf}} = 395$ GeV, the reduced couplings to b quarks and vector bosons have the opposite sign where the whole spectrum is identical. This reduced couplings can be, to some extent, identified with the coupling modifiers in the κ framework for SM Higgs studies, as pointed out in Sec. 2.1. This becomes more relevant in the following section, where we study a scenario with a very SM-like Higgs over the full μ_{inf} range.

The couplings to gauge bosons, especially the Z boson, also define the behaviour of the production cross section at a lepton collider like the ILC in the dominant production mode via Higgsstrahlung. We display in Fig. 4 how the cross section for $e^+e^- \rightarrow Zh_1$ evolves with μ_{inf} in this scenario for an initial center of mass energy $\sqrt{s} = 250$ GeV. Of course, the pure singlet case at $\mu_{\text{inf}} = 48$ GeV and 348 GeV cannot be produced. With a certain doublet admixture, however, a light singlet-like state can be produced at the ILC250 with a few femtobarn cross section. The coloured bands show the statistical uncertainties for integrated luminosities of $L = 100/\text{fb}$ (yellow) and $L = 2000/\text{fb}$ (green). The cross section uncertainty is derived as statistical uncertainty from a counting analysis:

$$\delta\sigma = \frac{\sigma}{\sqrt{N}} = \sqrt{\frac{\sigma}{L}}, \quad (20)$$

where the Poisson distribution defines the uncertainty from the number of signal events as \sqrt{N} .

Finally, we show the branching ratios for decays to bottom quarks and W boson pairs in Fig. 5. The light state h_1 mainly decays to bottom quarks over most of the displayed μ_{inf} range. Only at the points where it becomes exclusively singlet, the branching ratio to bottom quarks drops towards zero. For the second lightest state, the branching ratio to bottom quarks also goes down in the interval $125 \text{ GeV} \lesssim \mu_{\text{inf}} \lesssim 275 \text{ GeV}$, which is partially compensated by an increase in decays to W bosons. For a more detailed study of the behaviour, all decay modes have to be included. The rapid decrease of branching fractions of h_2 into both $b\bar{b}$ and W pairs at below $\mu_{\text{inf}} \simeq 750$ GeV is due to the opening of the $h_2 \rightarrow h_1h_1$ decay channel, where m_{h_2} becomes twice m_{h_1} . The displayed branching ratios of h_2 go down in the window around $\mu_{\text{inf}} \simeq 200$ GeV because here the decays into neutralinos and charginos become relevant (notice their corresponding small masses in this window). The two dips in $\text{Br}(h_2 \rightarrow W^+W^-)$ are due to an enhanced $\text{Br}(h_2 \rightarrow \tilde{\chi}_1^0\tilde{\chi}_2^0)$ in these regimes.

3.3 Reweighting μ_{inf} effects in the spectrum

It has been remarked in a previous study of the inflationary μ NMSSM, Ref. [5], that the neutralino spectrum at the tree level stays invariant under changes of μ_{inf} when the singlet self-coupling κ is adjusted appropriately. Under the same redefinition also the scalar spectrum does not change over vast regions in the parameter range aside from extreme configurations. Such an extreme case has been discussed in Ref. [5]. In the following, we refrain from artificial cancellations in the mass matrices and choose rather combinations of parameters to be constant such that variations in μ_{inf} enter mildly. From a quick study of the scalar mass matrix given in Eqs. (5), we see that three combinations are dominantly controlling the matrix elements. One is the sum $\mu_{\text{eff}} + \mu_{\text{inf}}$, then we have $\frac{\kappa}{\lambda}\mu_{\text{eff}}$ repeatedly appearing

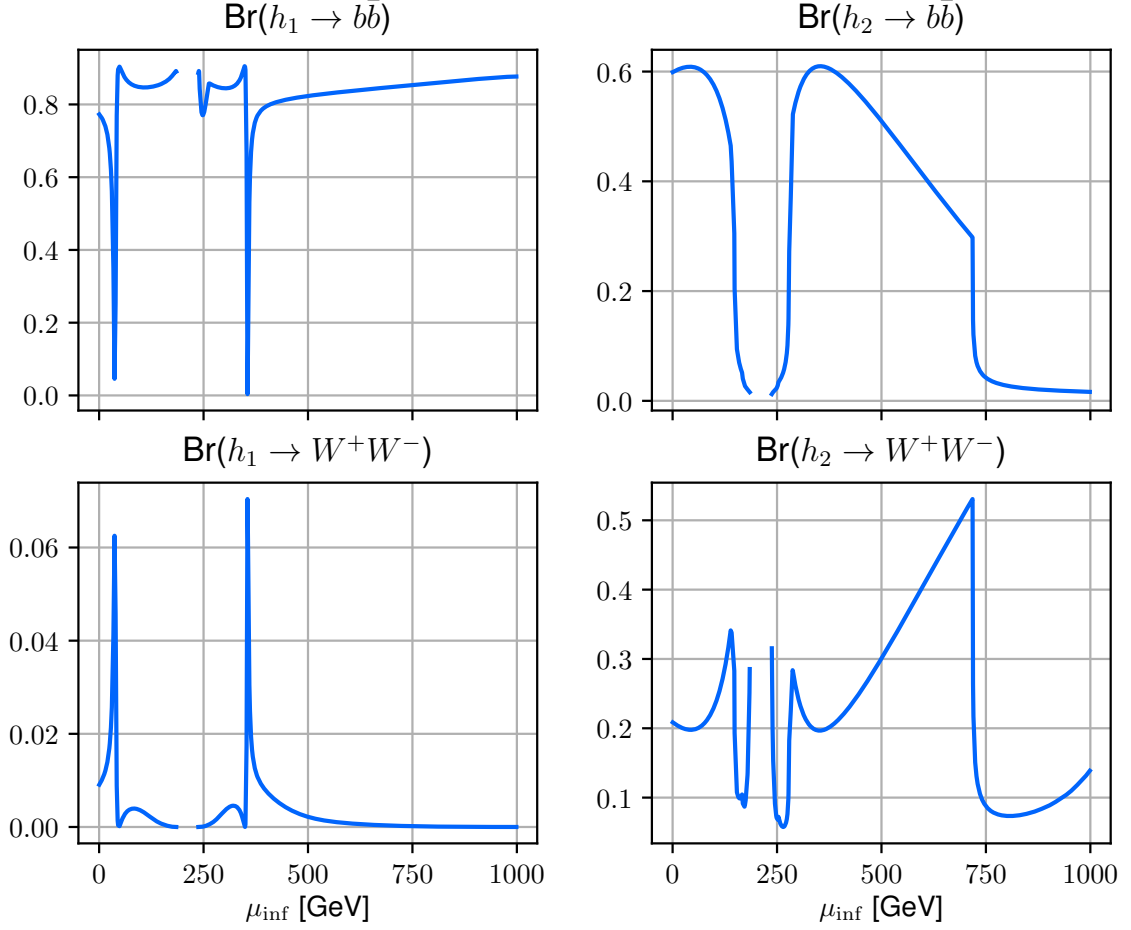


Figure 5: The branching ratios of h_1 and h_2 decay to b quarks or W bosons depending on μ_{inf}

and furthermore the combination that has been replaced by the charged Higgs mass dominating the heavy doublet mass eigenvalue.

We treat the following combinations constant under variation of μ_{inf} , which implies a redefinition of κ and μ_{eff} :

$$a = \mu_{\text{inf}} + \mu_{\text{eff}}, \quad (21a)$$

$$b = \frac{\kappa}{\lambda} \mu_{\text{eff}}, \quad (21b)$$

$$c = \mu_{\text{eff}} \left(\frac{\kappa}{\lambda} \mu_{\text{eff}} + A_\lambda \right) \equiv \frac{1}{2} (m_{H^\pm}^2 - m_W^2 + v^2 \lambda^2) \sin 2\beta. \quad (21c)$$

Keeping these combinations fixed, under variation of μ_{inf} the upper left blocks of the Higgs mass matrices are unchanged. The other mass matrix elements with a residual μ_{inf} dependence can then be

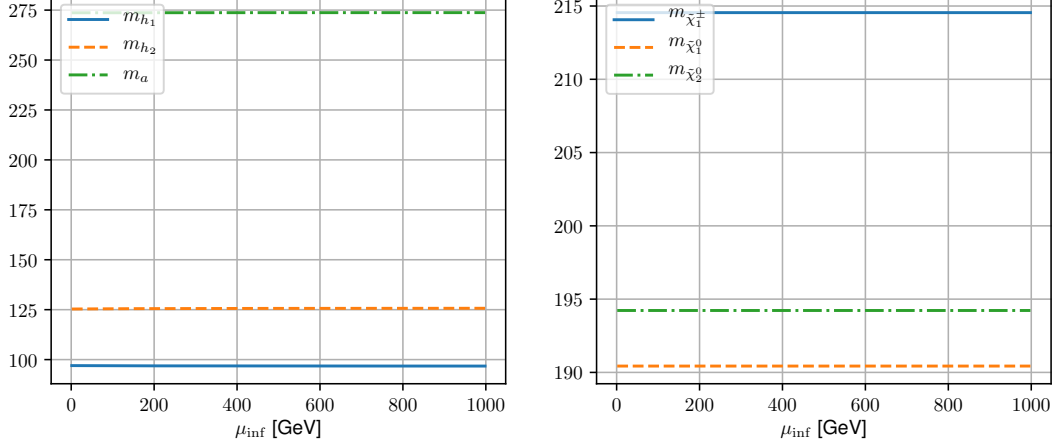


Figure 6: The masses of the light \mathcal{CP} -even states h_1 , h_2 , and the \mathcal{CP} -odd singlet-like state a (left); the masses of the light neutralinos $\tilde{\chi}_1^0$, $\tilde{\chi}_2^0$, and the light chargino $\tilde{\chi}_1^\pm$ (right), depending on the pure μ_{inf} effect.

expressed as

$$M_{S,33}^2 = \lambda^2 v^2 \left(\frac{\cos \beta \sin \beta}{a - \mu_{\text{inf}}} \left(\frac{c}{a - \mu_{\text{inf}}} - b \right) - \frac{\mu_{\text{inf}}}{a - \mu_{\text{inf}}} \right) + b(A_\kappa + 4b), \quad (22a)$$

$$M_{S,13}^2 = M_{S,31}^2 = v\lambda \left(2a \cos \beta - \left(\frac{c}{a - \mu_{\text{inf}}} + b \right) \sin \beta \right), \quad (22b)$$

$$M_{S,23}^2 = M_{S,32}^2 = v\lambda \left(2a \sin \beta - \left(\frac{c}{a - \mu_{\text{inf}}} + b \right) \cos \beta \right), \quad (22c)$$

and

$$M_{P,33}^2 = \lambda^2 v^2 \left(\frac{\cos \beta \sin \beta}{a - \mu_{\text{inf}}} \left(3b + \frac{c}{a - \mu_{\text{inf}}} \right) - \frac{\mu_{\text{inf}}}{a - \mu_{\text{inf}}} \right), \quad (23a)$$

$$M_{P,13}^2 = M_{P,31}^2 = -v\lambda \left(3b - \frac{c}{a - \mu_{\text{inf}}} \right) \sin \beta, \quad (23b)$$

$$M_{P,23}^2 = M_{P,32}^2 = -v\lambda \left(3b - \frac{c}{a - \mu_{\text{inf}}} \right) \cos \beta. \quad (23c)$$

Note, that the parameters λ , A_κ , and $\tan \beta$ can be essentially varied without changing the fixed combinations from above. Since we are studying the pure effect of μ_{inf} while minimally invasively changing the mass spectrum, we also keep them at the values specified in Tab. 3, where κ is not kept at that value. This can be seen also from Eqs. (22) and (23) where the appearance of κ is absorbed. The mass spectrum is then only slightly changing under increase of μ_{inf} from 0 GeV to 1000 GeV in contrast to what has been shown in Sec. 3.2. We show the correspondance of Fig. 1 in Fig. 6.

The question is now, how much the phenomenology of a μNMSSM point with large μ_{inf} differs from a point close to the NMSSM limit. Taking a look at the Higgs mixing components in Fig. 7, we see that the singlet admixture to the lightest state only mildly decreases. All changes in the mixings are less than at most 10...15%. It is interesting to notice that for increasing μ_{inf} , the doublet admixture to the lightest Higgs increases, where simultaneously the doublet components in h_2 become less relevant. Moreover, the larger μ_{inf} the less rapid the change.

The behaviour of the mixing components with respect to μ_{inf} is also mirrored in the reduced couplings

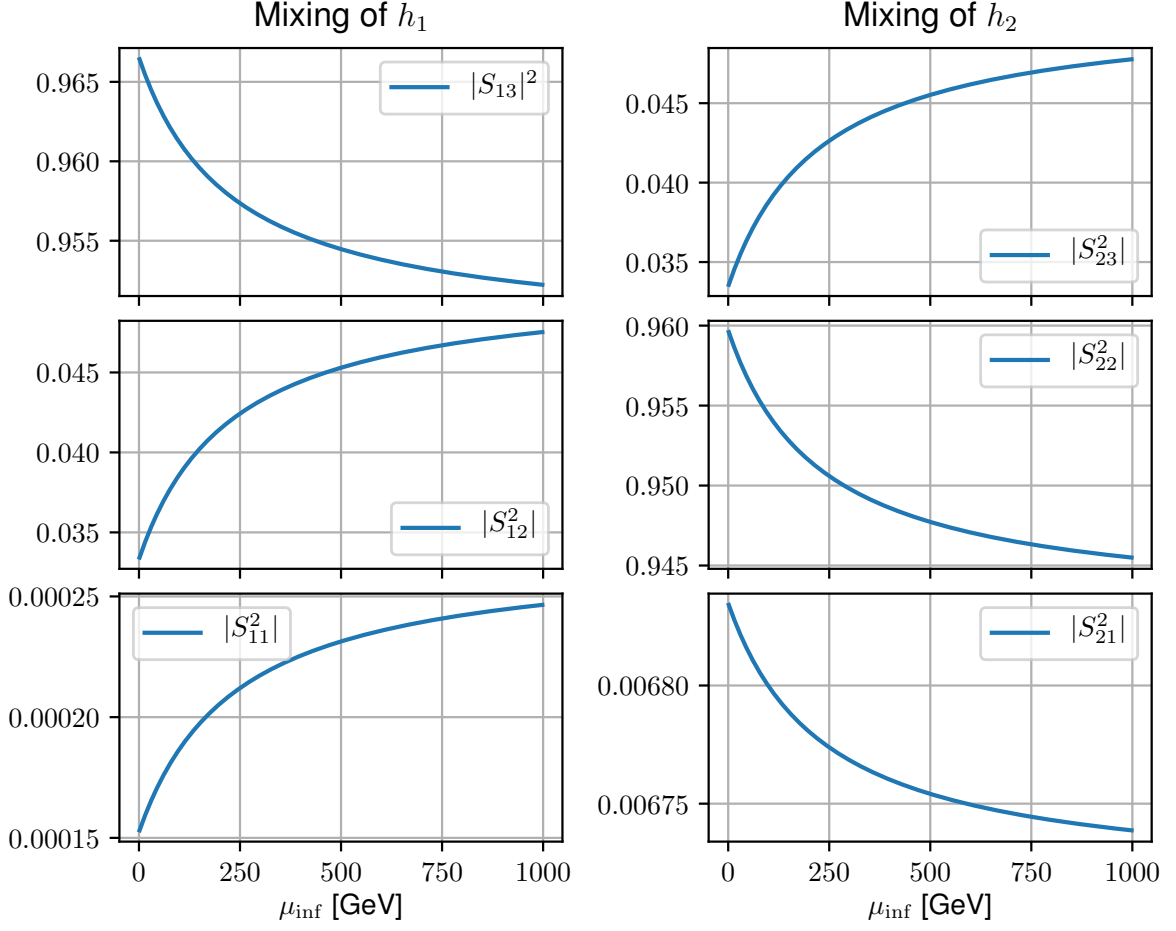


Figure 7: The three mixing components of the lightest scalar Higgs h_1 depending on the pure μ_{inf} effect. The down type component of h_1 is $|S_{11}|^2$, the up type component of h_1 is $|S_{12}|^2$ and the singlet component of h_1 is $|S_{13}|^2$

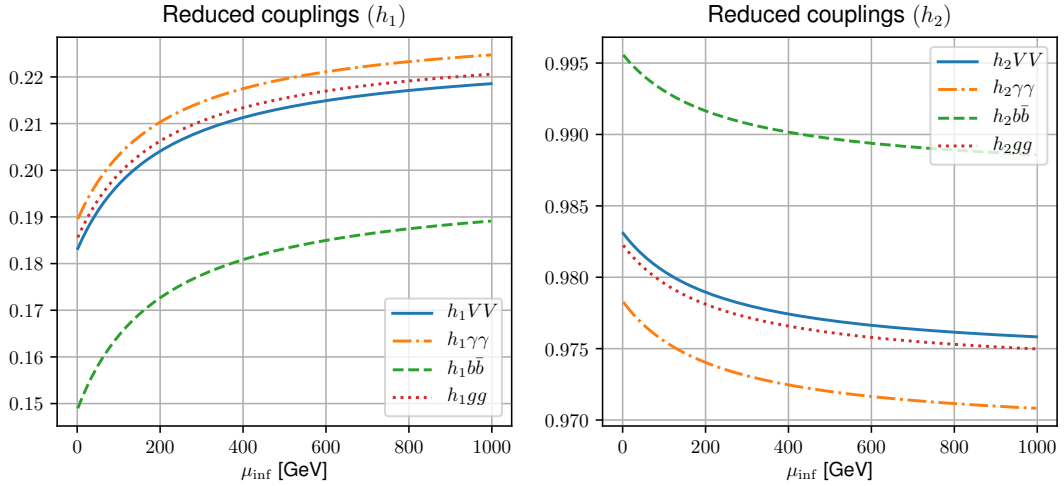


Figure 8: The reduced couplings of h_1 and h_2 to gauge bosons, photons, b quarks and gluons, depending on the pure μ_{inf} effect

shown in Fig. 8. Measuring a deviation of less than 2% from the SM-values for the SM-like scalar is more than challenging at the LHC and any future collider. Increasing μ_{inf} to around 1 TeV, we would have a deviation of less than 3% for the coupling to photons, where the bottom quark coupling of h_2 deviates only a bit more than 1% from the SM. Since for larger μ_{inf} the curves flatten out, a further increase of μ_{inf} in this scenario does not give a sizeable effect. On the other hand, the singlet-like scalar h_1 shows couplings of around 15 – 20% of a SM-Higgs at the same mass of 97 GeV. That means, if non-vanishing couplings can be measured to more than 10% at a future collider, there is a clear discovery potential for this singlet-like state. Nevertheless, it looks less promising to distinguish the μ NMSSM-scenario from the NMSSM point by just comparing the reduced couplings in the κ framework. If we look *e.g.* on the h_2 coupling to vector bosons in Fig. 8 (the blue continuous curve), which can be identified with κ_V , there is a variation of less than 0.01 over the displayed range. Supposed that at the ILC this κ_V can be measured to more than 1% accuracy [47], a deviation might be visible. The corresponding measurements of the signal strength for the singlet-like state, however, look more promising.

The same effect can also be seen in the total widths of h_1 and h_2 displayed in Fig. 9, where the curves follow the behaviour of the reduced couplings. Due to the rather small total width of the lightest Higgs boson, the effect of an increasing μ_{inf} is very prominent here, where the total width is nearly doubled over the displayed range. In contrast, for h_2 the total width is only mildly affected and its variation probably out of reach. Since we are on top of the SM-value for the total width around 4 MeV, see Refs. [26, 48], there is also not much room for invisible decay modes that are also not predicted in this scenario.

For a future study of this model at a collider, especially an e^+e^- machine, the production cross section of the singlet-dominated state is important. We calculate the cross section in Higgstrahlung at the ILC for a center of mass energy $\sqrt{s} = 250$ GeV as in Sec. 3.2. The result over the range $\mu_{\text{inf}} \in [0, 1000]$ GeV is shown in Fig. 10. Starting from the NMSSM benchmark point with $\mu_{\text{inf}} = 0$ GeV and a cross section of about 12.6 fb, the total cross section is enhanced by about 50% at $\mu_{\text{inf}} = 1000$ GeV. Already for $\mu_{\text{inf}} = 200$ GeV there is an increase of one quarter with respect to the initial cross section in the pure NMSSM scenario. In general, we want to stress that cross sections of more than 10 fb are well in reach for a linear collider [49–51]. A cross section enhanced by 50% compared to the NMSSM case is a clear sign of a possible distinction. The yellow and green coloured bands in Fig. 10 show the statistical uncertainties after an integrated luminosity of 100/fb and 2000/fb, respectively. The interpretation of these uncertainty bands is most useful when distinguishing two parameter points for different values μ_{inf} . At *e.g.* $\mu_{\text{inf}} = 200$ GeV the uncertainty band allows for cross sections between 15.2 and 16 fb with 100/fb of recorded data. Similarly, a cross section of 16 fb hints of a μ_{inf} in the range between 200 and 300 GeV. Nevertheless, for small values of μ_{inf} , the uncertainties are also smaller in absolute terms and a μ_{inf} of 50 GeV can be clearly distinguished from the $\mu_{\text{inf}} = 0$ GeV case. If we assume that the ILC can reach an integral luminosity of up to 2000/fb, the statistical uncertainty is narrowed down giving a much higher potential for distinction. In this case a measured cross section can be assigned to a smaller range of μ_{inf} and conversely larger values of μ_{inf} could be distinguished at the experiment. Note that we have considered the statistical error only for the displayed cross section, especially we did not consider the detection efficiency and possible backgrounds in the experimental study. However, we believe that the ILC at 250 GeV has a clear potential to distinguish the μ NMSSM from the NMSSM as well as certain scenarios within the same model and encourage further experimental studies including detector effects.

4 Conclusions

We have studied in detail the electroweak phenomenology of a supersymmetric model which incorporates inflation in the early universe. The model has the same particle content as the NMSSM and

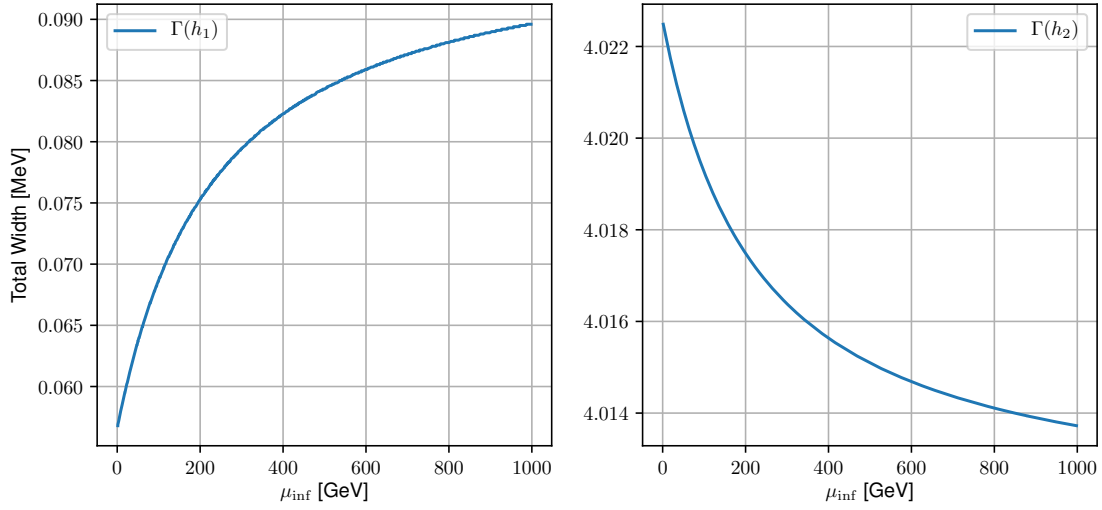


Figure 9: The total widths of the lightest scalar Higgs h_1 and second lightest Higgs h_2 depending on the pure μ_{inf} effect

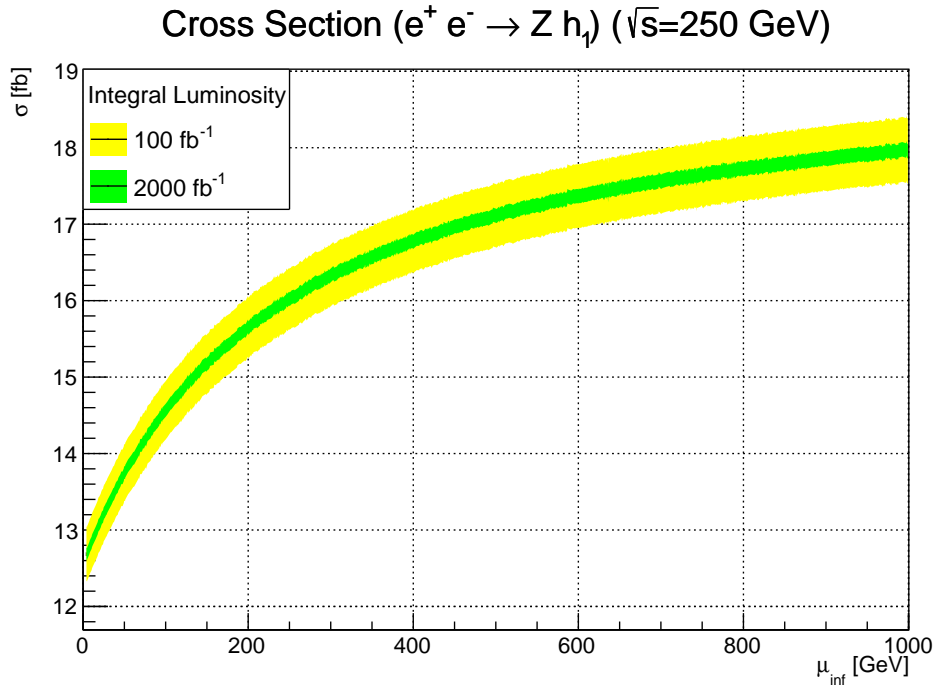


Figure 10: The lightest scalar Higgs production cross section at 250 GeV ILC depending on the pure μ_{inf} effect

comprises an additional singlet superfield. In contrast to the NMSSM, the speciality of our model is an additional μ -term like in the MSSM originating from the non-minimal coupling to gravity, leading to the so called μ NMSSM. Our study is focused on properties of the Higgs sector with a special emphasis on a light singlet-like state at 97 GeV. We have presented two routes how to distinguish a parameter point in the μ NMSSM—where μ_{inf} is the parameter relevant for inflation—from a corresponding parameter point in the NMSSM. The benchmark point in the NMSSM has been chosen from a random scan over NMSSM-specific parameters obeying all current experimental constraints.

For the numerical study, we have employed the public code collection `NMSSMTools` which serves as spectrum generator and calculates several observables. `NMSSMTools` does not provide the input options for the μ NMSSM, so we had to redefine the parameters in an appropriate way adopting the code for our model. We have identified a benchmark scenario to study the phenomenological differences of the NMSSM and the μ NMSSM. This benchmark scenario provides an allowed parameter point in the NMSSM, where we have checked against existing collider physics constraints by the use of `HiggsBounds/HiggsSignals` and `CheckMATE`. Starting from this valid point with $\mu_{\text{inf}} = 0$ GeV, we have studied the full effect of $\mu_{\text{inf}} \neq 0$ GeV to see how the spectrum and the mixing changes once this parameter is turned on. We have found a drastic influence on the mass spectrum, especially with one region where the lightest Higgs states turns to be tachyonic. Over the full range of μ_{inf} we have identified one more parameter point where the mass spectrum of Higgs bosons and neutralinos/charginos is degenerate with the NMSSM point. However, taking a look at the reduced couplings of the singlet-like state to electroweak gauge bosons and bottom quarks, we see a difference in the sign which may give a potential for disinction of the two models. Furthermore, we have calculated the production cross section of the lightest Higgs in Higgsstrahlung at the ILC with a center of mass energy $\sqrt{s} = 250$ GeV. For the relevant physical points it is around 10 fb and offers the possibility for a detailed study at the linear collider.

As a second route to study the “pure” μ_{inf} effect, we have reweighted other parameters to keep the mass spectrum invariant under variations of μ_{inf} . However, there is a sizeable effect on the Higgs mixing of a few percent and a reduction of the reduced couplings of the SM-like Higgs state to SM particles. Although the reduced couplings (or coupling-strength modifiers κ) deviate only by a few percent from the SM-value, such small deviations will be measureable at the future linear collider. In contrast, the singlet-like \mathcal{CP} -even state at 97 GeV receives enhanced contributions to the couplings to SM-particles due to an enhanced doublet admixture. Here, the change for increased μ_{inf} is more prominent with several percent. It is important to notice that the reduced couplings of the singlet-like state with respect to a SM-Higgs at 97 GeV are about 20% and therewith sufficiently large. The Higgsstrahlung cross section of the lightest Higgs at ILC250 is also increasing with increasing μ_{inf} reaching 18 fb in the scenario under scrutiny. This offers the possibility to distinguish the NMSSM and μ NMSSM scenarios from a measurement of the production cross section with sufficient integral luminosity.

Acknowledgments

We would like to thank Cyril Hugonie and Ulrich Ellwanger for their very helpful communication about the use of `NMSSMTools`. C.L., G.M.P, and S.P. acknowledge the support by the Deutsche Forschungsgemeinschaft (DFG German Research Association) under Germany’s Excellence Strategy –EXC 2121 “Quantum Universe”–390833306. W.G.H. is partially supported by the collaborative research center TRR 257 “Particle Physics Phenomenology after the Higgs Discovery”. We thank Sven Heinemeyer, Georg Weiglein, Stefan Liebler, Sebastian Paßehr for valuable discussions; furthermore, we thank Sven Heinemeyer and Sebastian Paßehr for a thorough read and comments on the manuscript.

References

- [1] M. B. Einhorn and D. R. T. Jones, “Inflation with Non-minimal Gravitational Couplings in Supergravity”, *JHEP* 03 (2010) 026, [arXiv:0912.2718 \[hep-ph\]](#). [pp 2, 3]
- [2] S. Ferrara, R. Kallosh, A. Linde, A. Marrani, and A. Van Proeyen, “Jordan Frame Supergravity and Inflation in NMSSM”, *Phys. Rev. D* 82 (2010) 045003, [arXiv:1004.0712 \[hep-th\]](#). [pp 2, 3]
- [3] S. Ferrara, R. Kallosh, A. Linde, A. Marrani, and A. Van Proeyen, “Superconformal Symmetry, NMSSM, and Inflation”, *Phys. Rev. D* 83 (2011) 025008, [arXiv:1008.2942 \[hep-th\]](#). [pp 2, 3, 4]
- [4] H. M. Lee, “Chaotic inflation in Jordan frame supergravity”, *JCAP* 1008 (2010) 003, [arXiv:1005.2735 \[hep-ph\]](#). [pp 2, 3, 4]
- [5] W. G. Hollik, S. Liebler, G. Moortgat-Pick, S. Paßehr, and G. Weiglein, “Phenomenology of the inflation-inspired NMSSM at the electroweak scale”, *Eur. Phys. J. C* 79 no. 1, (2019) 75, [arXiv:1809.07371 \[hep-ph\]](#). [pp 2, 3, 4, 7, 13]
- [6] OPAL, G. Abbiendi *et al.*, “Decay mode independent searches for new scalar bosons with the OPAL detector at LEP”, *Eur. Phys. J. C* 27 (2003) 311–329, [arXiv:hep-ex/0206022](#). [p 2]
- [7] LEP Working Group for Higgs boson searches, ALEPH, DELPHI, L3, OPAL, R. Barate *et al.*, “Search for the standard model Higgs boson at LEP”, *Phys. Lett. B* 565 (2003) 61–75, [arXiv:hep-ex/0306033](#). [p 2]
- [8] ALEPH, DELPHI, L3, OPAL, LEP Working Group for Higgs Boson Searches, S. Schael *et al.*, “Search for neutral MSSM Higgs bosons at LEP”, *Eur. Phys. J. C* 47 (2006) 547–587, [arXiv:hep-ex/0602042 \[hep-ex\]](#). [p 2]
- [9] CMS, A. M. Sirunyan *et al.*, “Search for a standard model-like Higgs boson in the mass range between 70 and 110 GeV in the diphoton final state in proton-proton collisions at $\sqrt{s} = 8$ and 13 TeV”, *Phys. Lett. B* 793 (2019) 320–347, [arXiv:1811.08459 \[hep-ex\]](#). [p 2]
- [10] CMS, A. M. Sirunyan *et al.*, “Search for additional neutral MSSM Higgs bosons in the $\tau\tau$ final state in proton-proton collisions at $\sqrt{s} = 13$ TeV”, *JHEP* 09 (2018) 007, [arXiv:1803.06553 \[hep-ex\]](#). [p 2]
- [11] ATLAS, The ATLAS collaboration, “Search for resonances in the 65 to 110 GeV diphoton invariant mass range using 80 fb^{-1} of pp collisions collected at $\sqrt{s} = 13$ TeV with the ATLAS detector”,. [p 2]
- [12] R. Dermisek and J. F. Gunion, “A Comparison of Mixed-Higgs Scenarios In the NMSSM and the MSSM”, *Phys. Rev. D* 77 (2008) 015013, [arXiv:0709.2269 \[hep-ph\]](#). [p 2]
- [13] G. Belanger, U. Ellwanger, J. F. Gunion, Y. Jiang, S. Kraml, and J. H. Schwarz, “Higgs Bosons at 98 and 125 GeV at LEP and the LHC”, *JHEP* 01 (2013) 069, [arXiv:1210.1976 \[hep-ph\]](#). [p 2]
- [14] J. Cao, X. Guo, Y. He, P. Wu, and Y. Zhang, “Diphoton signal of the light Higgs boson in natural NMSSM”, *Phys. Rev. D* 95 no. 11, (2017) 116001, [arXiv:1612.08522 \[hep-ph\]](#). [p 2]
- [15] F. Domingo, S. Heinemeyer, S. Paßehr, and G. Weiglein, “Decays of the neutral Higgs bosons into SM fermions and gauge bosons in the CP -violating NMSSM”, *Eur. Phys. J. C* 78 no. 11, (2018) 942, [arXiv:1807.06322 \[hep-ph\]](#). [p 2]
- [16] T. Biekötter, S. Heinemeyer, and C. Muñoz, “Precise prediction for the Higgs-boson masses in the $\mu\nu$ SSM”, *Eur. Phys. J. C* 78 no. 6, (2018) 504, [arXiv:1712.07475 \[hep-ph\]](#). [p 2]
- [17] T. Biekötter, M. Chakraborti, and S. Heinemeyer, “A 96 GeV Higgs boson in the N2HDM”, *Eur. Phys. J. C* 80 no. 1, (2020) 2, [arXiv:1903.11661 \[hep-ph\]](#). [p 2]
- [18] T. Biekötter, S. Heinemeyer, and C. Muñoz, “Precise prediction for the Higgs-Boson masses in the $\mu\nu$ SSM with three right-handed neutrino superfields”, *Eur. Phys. J. C* 79 no. 8, (2019) 667, [arXiv:1906.06173 \[hep-ph\]](#). [p 2]
- [19] J. Cao, X. Jia, Y. Yue, H. Zhou, and P. Zhu, “96 GeV diphoton excess in seesaw extensions of the natural NMSSM”, *Phys. Rev. D* 101 no. 5, (2020) 055008, [arXiv:1908.07206 \[hep-ph\]](#). [p 2]
- [20] K. Choi, S. H. Im, K. S. Jeong, and C. B. Park, “Light Higgs bosons in the general NMSSM”, *Eur. Phys. J. C* 79 no. 11, (2019) 956, [arXiv:1906.03389 \[hep-ph\]](#). [p 2]
- [21] F. Richard, “Indications for extra scalars at LHC? – BSM physics at future e^+e^- colliders”, [arXiv:2001.04770 \[hep-ex\]](#). [p 2]
- [22] J. A. Aguilar-Saavedra and F. R. Joaquim, “Multiphoton signals of a (96 GeV?) stealth boson”, [arXiv:2002.07697 \[hep-ph\]](#). [p 2]
- [23] T. Biekötter, M. Chakraborti, and S. Heinemeyer, “The ’96 GeV excess’ at the LHC”, 3, 2020. [arXiv:2003.05422 \[hep-ph\]](#). [p 2]
- [24] U. Ellwanger and M. Rodriguez-Vazquez, “Discovery Prospects of a Light Scalar in the NMSSM”, *JHEP* 02 (2016) 096, [arXiv:1512.04281 \[hep-ph\]](#). [p 2]
- [25] U. Ellwanger, C. Hugonie, and A. M. Teixeira, “The Next-to-Minimal Supersymmetric Standard Model”, *Phys. Rept.* 496 (2010) 1–77, [arXiv:0910.1785 \[hep-ph\]](#). [pp 3, 7]
- [26] LHC Higgs Cross Section Working Group, J. R. Andersen *et al.*, “Handbook of LHC Higgs Cross Sections: 3. Higgs Properties”, [arXiv:1307.1347 \[hep-ph\]](#). [pp 6, 17]
- [27] U. Ellwanger, J. F. Gunion, and C. Hugonie, “NMHDECAY: A Fortran code for the Higgs masses, couplings and decay widths in the NMSSM”, *JHEP* 02 (2005) 066, [arXiv:hep-ph/0406215 \[hep-ph\]](#). [pp 6, 8]
- [28] U. Ellwanger and C. Hugonie, “NMSPEC: A Fortran code for the sparticle and Higgs masses in the NMSSM with GUT scale boundary conditions”, *Comput. Phys. Commun.* 177 (2007) 399–407, [arXiv:hep-ph/0612134 \[hep-ph\]](#). [pp 6, 8]
- [29] D. Das, U. Ellwanger, and A. M. Teixeira, “NMSDECAY: A Fortran Code for Supersymmetric Particle Decays in the Next-to-Minimal Supersymmetric Standard Model”, *Comput. Phys. Commun.* 183 (2012) 774–779, [arXiv:1106.5633 \[hep-ph\]](#). [p 6]
- [30] F. Domingo, “A New Tool for the study of the CP -violating NMSSM”, *JHEP* 06 (2015) 052, [arXiv:1503.07087 \[hep-ph\]](#). [p 6]
- [31] See: <https://www.lupm.in2p3.fr/users/nmssm/README>. [p 6]

- [32] U. Ellwanger and C. Hugonie, “NMHDECAY 2.0: An Updated program for sparticle masses, Higgs masses, couplings and decay widths in the NMSSM”, *Comput. Phys. Commun.* **175** (2006) 290–303, [arXiv:hep-ph/0508022](#). [p 8]
- [33] P. Bechtle, O. Brein, S. Heinemeyer, G. Weiglein, and K. E. Williams, “HiggsBounds: Confronting Arbitrary Higgs Sectors with Exclusion Bounds from LEP and the Tevatron”, *Comput. Phys. Commun.* **181** (2010) 138–167, [arXiv:0811.4169 \[hep-ph\]](#). [p 8]
- [34] P. Bechtle, O. Brein, S. Heinemeyer, O. Stål, T. Stefaniak, G. Weiglein, and K. E. Williams, “HiggsBounds – 4: Improved Tests of Extended Higgs Sectors against Exclusion Bounds from LEP, the Tevatron and the LHC”, *Eur. Phys. J. C* **74** no. 3, (2014) 2693, [arXiv:1311.0055 \[hep-ph\]](#). [p 8]
- [35] P. Bechtle, S. Heinemeyer, O. Stål, T. Stefaniak, and G. Weiglein, “HiggsSignals: Confronting arbitrary Higgs sectors with measurements at the Tevatron and the LHC”, *Eur. Phys. J. C* **74** no. 2, (2014) 2711, [arXiv:1305.1933 \[hep-ph\]](#). [p 8]
- [36] O. Stål and T. Stefaniak, “Constraining extended Higgs sectors with HiggsSignals”, *PoS EPS-HEP2013* (2013) 314, [arXiv:1310.4039 \[hep-ph\]](#). [p 8]
- [37] DELPHES 3, J. de Favereau, C. Delaere, P. Demin, A. Giammanco, V. Lemaitre, A. Mertens, and M. Selvaggi, “DELPHES 3, A modular framework for fast simulation of a generic collider experiment”, *JHEP* **02** (2014) 057, [arXiv:1307.6346 \[hep-ex\]](#). [p 8]
- [38] M. Cacciari, G. P. Salam, and G. Soyez, “FastJet User Manual”, *Eur. Phys. J. C* **72** (2012) 1896, [arXiv:1111.6097 \[hep-ph\]](#). [p 8]
- [39] M. Cacciari and G. P. Salam, “Dispelling the N^3 myth for the k_t jet-finder”, *Phys. Lett. B* **641** (2006) 57–61, [arXiv:hep-ph/0512210](#). [p 8]
- [40] M. Cacciari, G. P. Salam, and G. Soyez, “The anti- k_t jet clustering algorithm”, *JHEP* **04** (2008) 063, [arXiv:0802.1189 \[hep-ph\]](#). [p 8]
- [41] A. L. Read, “Presentation of search results: The CL(s) technique”, *J. Phys. G* **28** (2002) 2693–2704. [p 8]
- [42] M. Drees, H. Dreiner, D. Schmeier, J. Tattersall, and J. S. Kim, “CheckMATE: Confronting your Favourite New Physics Model with LHC Data”, *Comput. Phys. Commun.* **187** (2015) 227–265, [arXiv:1312.2591 \[hep-ph\]](#). [p 8]
- [43] D. Dercks, N. Desai, J. S. Kim, K. Rolbiecki, J. Tattersall, and T. Weber, “CheckMATE 2: From the model to the limit”, *Comput. Phys. Commun.* **221** (2017) 383–418, [arXiv:1611.09856 \[hep-ph\]](#). [p 8]
- [44] G. Belanger, F. Boudjema, A. Pukhov, and A. Semenov, “MicrOMEGAs: A Program for calculating the relic density in the MSSM”, *Comput. Phys. Commun.* **149** (2002) 103–120, [arXiv:hep-ph/0112278](#). [p 9]
- [45] G. Belanger, F. Boudjema, A. Pukhov, and A. Semenov, “MicrOMEGAs 2.0: A Program to calculate the relic density of dark matter in a generic model”, *Comput. Phys. Commun.* **176** (2007) 367–382, [arXiv:hep-ph/0607059](#). [p 9]
- [46] G. Belanger, F. Boudjema, A. Pukhov, and A. Semenov, “micrOMEGAs_3: A program for calculating dark matter observables”, *Comput. Phys. Commun.* **185** (2014) 960–985, [arXiv:1305.0237 \[hep-ph\]](#). [p 9]
- [47] H. Bahl *et al.* BONN-TH 2019-04, DESY 19-093, KA-TP-09-2019, IFT-UAM/CSIC-19-075, to be published, private communication with S. Heinemeyer. [p 17]
- [48] LHC Higgs Cross Section Working Group, D. de Florian *et al.*, “Handbook of LHC Higgs Cross Sections: 4. Deciphering the Nature of the Higgs Sector”, [arXiv:1610.07922 \[hep-ph\]](#). [p 17]
- [49] K. Fujii *et al.*, “The Potential of the ILC for Discovering New Particles”, [arXiv:1702.05333 \[hep-ph\]](#). [p 17]
- [50] A. Arbey *et al.*, “Physics at the e^+e^- Linear Collider”, *Eur. Phys. J. C* **75** no. 8, (2015) 371, [arXiv:1504.01726 \[hep-ph\]](#). [p 17]
- [51] H. Baer, T. Barklow, K. Fujii, Y. Gao, A. Hoang, S. Kanemura, J. List, H. E. Logan, A. Nomerotski, M. Perelstein, *et al.*, “The International Linear Collider Technical Design Report - Volume 2: Physics”, [arXiv:1306.6352 \[hep-ph\]](#). [p 17]